Journal of Industrial Microbiology & Biotechnology (2001) 26, 77–82

www.nature.com/jim

Nuclear magnetic resonance imaging (MRI) of diesel oil migration in estuarine sediment samples

AD Reeves[1] and JA Chudek[2]

[1]*Geography Department, University of Dundee, Dundee DD1 4HN, UK;* [2]*Chemistry Department, University of Dundee, Dundee DD1 4HN, UK*

Magnetic resonance imaging (MRI) provides a means of monitoring the change in position and the eventual breakdown of oil within sediments. The multidimensional technique allows the position of nuclei (most commonly protons) to be located within a known volume of substrate, e.g. sediment, hence offering a method of assessing the harming potential of oils in near-shore environments. Two-dimensional (2D) and three-dimensional (3D) MRI analyses of the measurement and movement of oil in estuarine sediments show that, using appropriate parameters, movement of the oil can be both observed and quantified. To aid the quantification a sample holder fabricated from polyvinylsiloxane, an inert material visible in magnetic resonance images has been used as an internal intensity standard. The results show the great potential of MRI in studying protonated contaminants in these materials, notwithstanding the presence of paramagnetic species in estuarine sediments which might distort the image. Sediments studied thus far have been collected from the Tay Estuary, Northeast Scotland. *Journal of Industrial Microbiology & Biotechnology* (2001) **26,** 77–82.

Keywords: NMR imaging; oil; migration rates; estuarine sediments; Tay Estuary

Introduction

Magnetic resonance imaging (MRI) is used widely in hospitals as a diagnostic tool allowing medical practitioners to observe the internal organs of patients. This technique, which is a direct development of nuclear magnetic resonance (NMR) spectroscopy, has considerable potential in a wide range of applications related to environmental science [19]. In the present study, magnets of considerably greater field strength and with a smaller bore than those found in hospitals were used; this allowed samples to be imaged to a much higher resolution, potentially pixels or voxels down to between 5 and 10 μm on a side compared to the 5 mm typically attained by conventional MRI [15]. Work similar to that reported here could, in fact, be carried out in such a hospital MRI set up. MRI is non-invasive and non-destructive. Its use allows specimens to be re-examined over time or after treatment (e.g. after the addition of pollutants). As its name implies, NMR spectroscopy measures the interactions of atomic nuclei with magnetic fields. Different atomic nuclei have different nuclear spins and when a powerful magnetic field is applied, these nuclear spins align themselves to the field in a finite number of allowed orientations. Applying a force can perturb these orientations, e.g. from a burst of radio frequency (rf) energy from which the energy needed to cause the perturbation is absorbed. After initial absorption, the energy is retransmitted again as rf as the nuclei relax. It is this re-transmitted rf which is detected. Although the nuclei of many isotopes can theoretically be imaged, sensitivity restraints limit the range to a select few of which the hydrogen nucleus (^{1}H) is, by far, the most commonly observed. Intra- and intermolecular interactions, along with the strength of the applied magnetic field, determine the frequency at which energy is absorbed. In a uniform field, therefore, moieties of the same type, in equivalent environments, will absorb energy (or resonate) at the same frequency. The superimposition of a linear magnetic field gradient on the original field introduces a spatial dimension and the nuclei (here ^{1}H) — chemically equivalent but physically separated along the gradient — will resonate at a frequency governed by the strength of the gradient and their respective positions. By applying three orthogonal field gradients, it is possible to generate a three-dimensional (3D) map of the distribution of the protons. The density of ^{1}H, moderated by restraints imposed by their physical and chemical environment, dictates the intensity of the signal [4]. Image intensity and contrast are further dependent on image acquisition parameters, which can be varied to highlight different features within the sample. Thus, a MR image of oil in sediment shows bright areas corresponding to the area in which oil is present; this area, or volume, can be accurately measured and, by running consecutive images, the direction and rate of diffusion measured. The level of intensity is proportional to the local oil concentration. Much work relating to the determination of fluid flow (water and oil) has been undertaken on oil-bearing strata particularly in the sphere of oil well logging [1,10,17,18,20,25,35,36].

At present, most geophysical applications of NMR relate to the study of dispersive flow in model or representative systems, usually porous media, including the study of particles forming chromatography beds [2,3,6–9,13,16,21–24,26,27,32,33,34].

Applications in the field of environmental science and engineering, particularly biodegradation, biotransformation and contaminant retardation, are becoming more common [6,11,12,19]. In marine science, progress is limited to structural characterisation; e.g. humic acids in marine sediments using C-13 NMR [31]. Imaging liquids in sediments has until recently been thought to be very difficult, if not impossible. It has now been shown [5,29] that with suitable parameters, both the presence of protonic impurities and their movement in sediments can be observed. The potential of

Correspondence: Dr AD Reeves, Geography Department, University of Dundee, Dundee DD1 4HN, UK
Received 26 January 2000; accepted 7 June 2000

Table 1 Image intensity measured for different volumes of oil added

Amount of oil added	Intensity
Dry	3.39×10^4 (background noise level)
400 μl	3.53×10^4
800 μl	3.61×10^4
1600 μl	3.85×10^4

Intensities are averages of duplicate samples.

using MRI in the characterisation and diagnostics of hydrocarbon-contaminated soils using simulated porous media has been examined [28]. Imaging was based on hydrogen nuclei MR signals detecting water and hydrocarbon-rich liquids (e.g. TCE; trichloroethylene) residing in pore spaces. NMR spectroscopy is also being successfully applied to the study of hydrophobicity in oil-contaminated soils [30] and to soil organic matter content [14].

In sediments, a range of factors influences image acquisition; many of these lead to localized distortion of the applied magnetic field and field gradients. The effects of air spaces, liquid/air and liquid/liquid interfaces on the homogeneity of the magnetic field can be negated by using a two-pulse acquisition sequence which refocuses the magnetization in a time equal to twice the gap between the pulses (this is known as the time to echo, TE). Another factor influencing image acquisition is the effect of paramagnetic species within the mineral structure of the sediment on the relaxation time (the time taken for the nuclei to retransmit absorbed rf, T_2) of the excited nuclei.

Where the concentration of paramagnetic species is high, T_2 can be very short, and if TE is long compared to T_2, then the signal will totally decay before it can be collected. In order to make this method quantitative, it is necessary to include a reference in close proximity to the sample being measured, the image intensity of which will act as a standard against which the intensity of the image of the contaminated material might be measured and quantified.

In the series of experiments reported here, 3D images of samples of sediment, contaminated and uncontaminated, were obtained. The samples were held in a container made of polyvinylsiloxane. Polyvinylsiloxane is visible using MRI and thus fulfills a dual role as holder and reference.

Under normal conditions, the main requirement of MRI is to produce an image at the best resolution available. This can be time-consuming. In these experiments, quantification of contaminant distribution, measured in the shortest possible time, was considered paramount. In an imaging experiment, it is necessary to acquire a two-dimensional (2D) data array or a 3D data array to produce 2D and 3D images, respectively. Taken in the simplest terms, to collect data for a $128\times128\times128$ voxel image, a matrix of $256\times128\times128$ data points must be constructed. All 256 points in the read direction are collected serially in a very short time; however, to maintain resolution, this must be collected 128×128 times. It was decided that in order to minimize acquisition time, resolution would be kept to a maximum in the gravity-driven direction but reduced in the other two. Consequently, data were collected into $256\times32\times32$ matrices, reducing the acquisition time by a factor of 16.

Making use of this method of data acquisition, the movement of oil down a column of sediment was followed over a 72-h period.

Table 2 Sediment characteristics

Loss on ignition (2 h at 800°C): 2.05%
Coulter LS230 laser analysis: 75.2% sand, 23.3% silt, 1.5% clay

Table 3 Acquisition parameters

Sweep width	125,000 Hz
Pulse width	10 μs (90°)
Repetition time	1 s
Echo time	2.35 ms
Field of view	$(30\ \text{mm})^3$
Sample AR35 Figures 1–3	
Matrix size	$(128)^3$
Voxel size	$(240\ \mu\text{m})^3$
Sample AR31 Figure 4; *sample AR37* Figure 8	
Matrix size	$128\times32\times32$
Voxel size	$240\times980\times980\ \mu\text{m}^3$

Materials and methods

Sample collection and handling

Sediments were sampled from a site at Invergowrie Bay (Grid ref. OS 357 297) using a grab sampler of modified van Veen design (0.25 m^3 volume) with added teeth to collect material more effectively (commissioned by the Tay Estuary Research Center). The grab penetrates bottom sediments to a depth of 10 cm. Samples were collected, returned to the laboratory, and air-dried for immediate use.

Subsamples were examined in the MR imager with no pre-preparation. An inert polyvinylsiloxane sample holder (Coltene

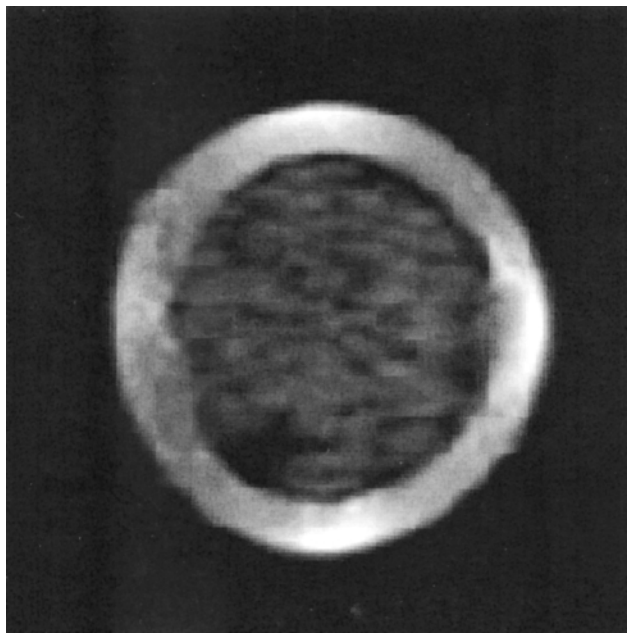

Figure 1 Transverse slice; air-dried sediment saturated with diesel oil.

President Impression Material; 23 mm×17 mm i.d.) was filled with artificially contaminated sediment (Granville diesel oil 15 W/40). An aliquot of oil (Table 1) was added to the sediment. The sample holder was subsequently placed in a 25-mm o.d. glass tube and inserted into the magnet. Image data collection was started immediately. Sediment characteristics were determined using a Coulter Particle Size Analyser LS 230 (Table 2).

NMR imaging experiments

NMR images were accumulated on a Bruker AM300/WB FT NMR spectrometer fitted with a Bruker Microimaging probe using a 25-mm saddle resonator.

Imaging data were accumulated using a standard Bruker 3D spin echo sequence (XYSE3D). By keeping the time to echo (TE) to <4 ms, it was possible to image oil in marine sediments containing 3% Fe. Acquisition parameters are given in Table 3.

Results

Figure 1 shows a transverse slice out of a 128 voxel^3 image (interpolated to 192 voxel^3) of the polyvinylsiloxane container with a sample of air-dried sediment saturated with diesel oil. Both the container and the diesel oil in the sediment can be seen in the image; the slight distortions in the intensity of the container are almost certainly due to the effects of paramagnetic materials in the sediment. Figures 2 and 3 show a longitudinal view of a maximum intensity projection through the full 3D data set from which the slice shown in Figure 1 was extracted, and a longitudinal view of an electronically sliced surface-rendered reconstruction from the same data set, respectively. In the case of the latter, a range of grey levels representing the container and a range representing higher levels of contamination were selected. Figure 2 shows signs of the effects of paramagnetism. This highlights a secondary role of the reference material, in that the effects of the paramagnetic materials in the sediment are observable and serve as an indicator of their strength. In Figure 3, the distribution of oil density is instantly observable. As can be seen, oil has concentrated near the top, the bottom and down one side. The oil was originally evenly distributed through the sample and this shows the position after 36 h.

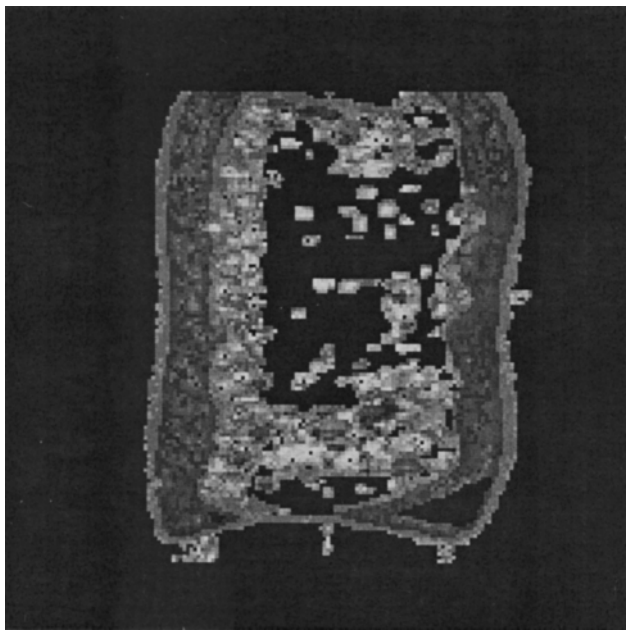

Figure 3 Longitudinal view of surface-rendered projection of Figure 1.

The image shown in Figure 4 is of sediment containing 800 μl diesel oil; these data were collected as an 128×32×32 matrix which gives maximum resolution along the longitudinal axis only. This data set was collected in only 1 h. It allows sufficient information on concentration and movement to be collected in a

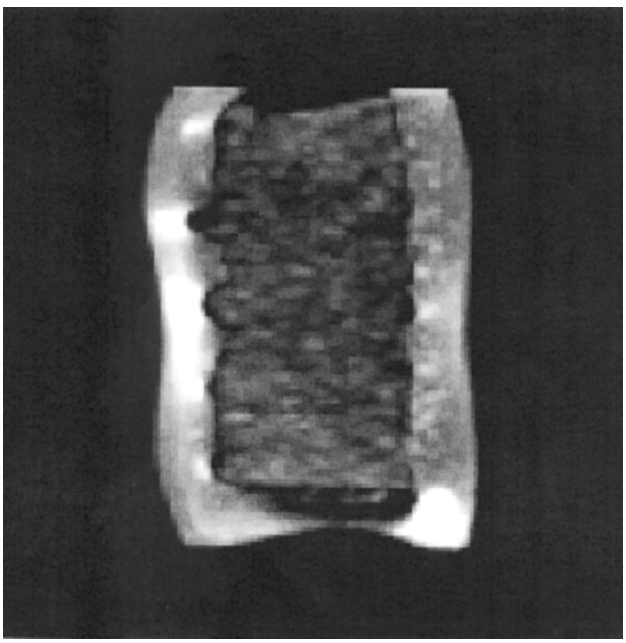

Figure 2 Longitudinal view of maximum intensity projection of Figure 1.

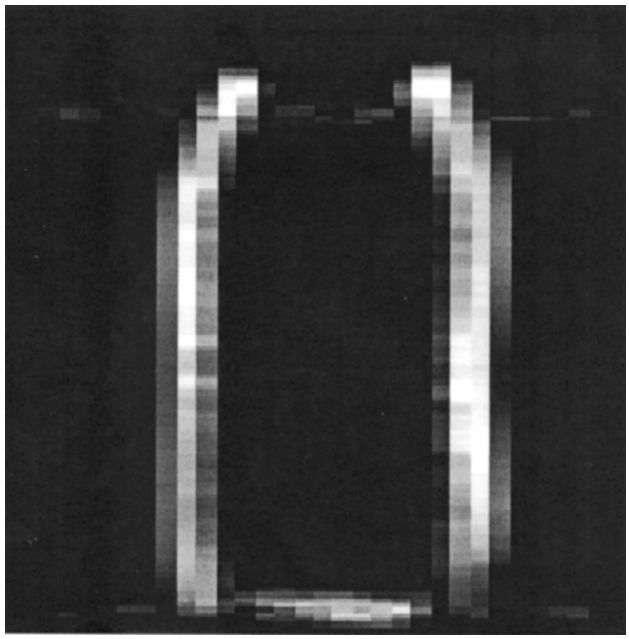

Figure 4 Air-dried sediment with 800 μl diesel oil added.

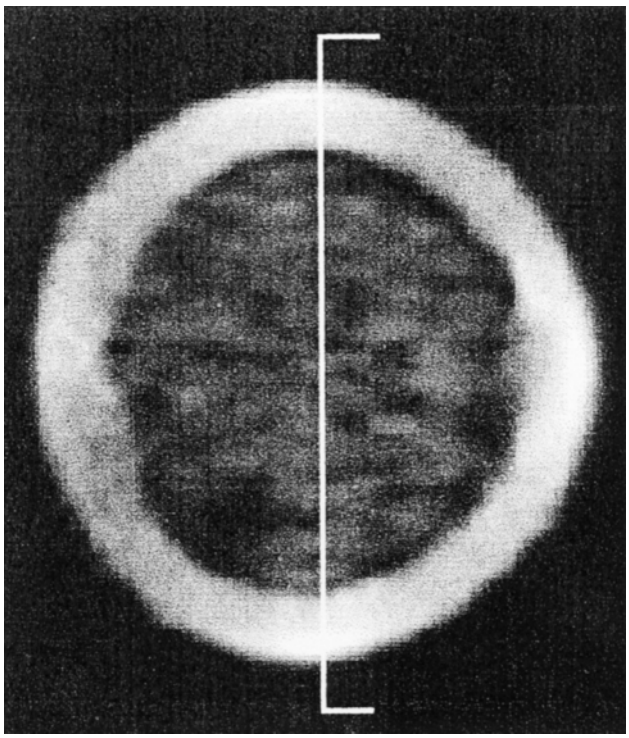

Figure 5 Image showing position of section used to calculate variations in pixel intensity across a sample.

short time. The 128 voxel^3 images shown in the other figures (Figures 1–3) took 36 h to collect. As an indication of the ability to quantify intensities, Figure 6 shows an intensity profile through the slice in Figure 5. Modern software also allows integration of intensities over variable areas of the image (not shown). Using the acquisition parameters for images, such as that in Figure 4, a series of samples with different concentrations of oil was imaged. The area of the sediment was integrated for each image and the intensity, when plotted, gave a linear calibration curve (Table 1 and Figure 7). This again demonstrates the quantitative nature of these experiments.

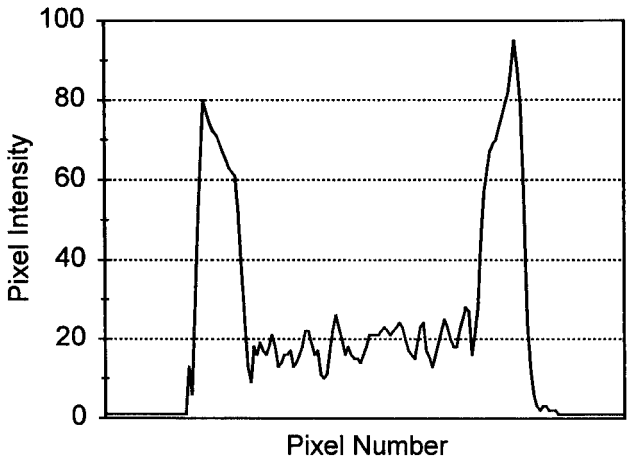

Figure 6 Graph to show variation in pixel intensity through a contaminated sediment. Pixel numbers range from 0 to 192.

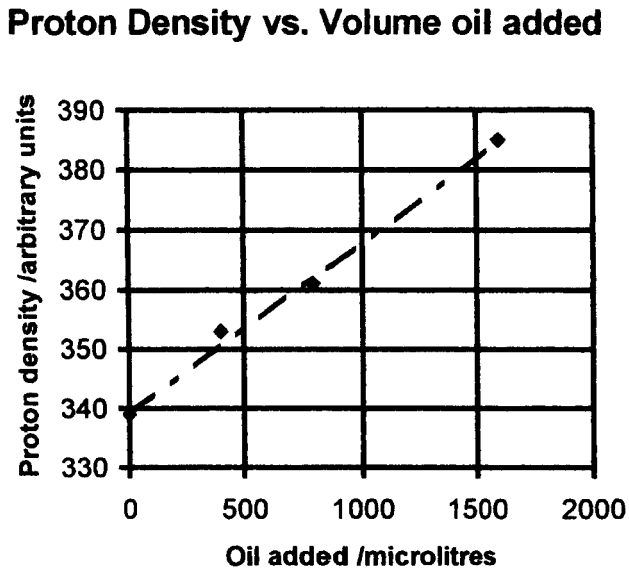

Figure 7 Graph to show measured proton density in arbitrary units vs. volume of oil added to the sediment sample.

Intensity profiles collected from the centre of a plug of sediment in the sample holder are shown in Figure 8. Trace A shows the penetration of oil during the first hour after addition, trace B after 36 h and trace C after 72 h.

Discussion

The distribution of oil in the polyvinylsiloxane container can be seen clearly in Figures 1 and 2. There are some distortions: the image intensity of the container is not completely uniform in the lateral slice, while in Figure 2, the overall shape of the container is distorted slightly (this is clearer in Figure 3, a surface reconstruction of the full 3D data set cut in half to show the outline of the container). There are several possible reasons for these effects. The intensity changes could be due to the size of the sample. Samples, which completely fill the resonator, can affect the applied rf, leading to changes in the intensity of images. These distortions usually involve two areas of increased intensity diametrically opposite to each other. Distortion of the shape can simply be the result of a badly set up instrument, but is more likely to be the effect of paramagnetic materials in the sediment coupled with susceptibility effects. Close examination of the images indicates that the latter could be the cause of the distortions. In Figure 1, there is a slight streaking (left to right) in the image of the oil. In Figure 2, the top corner of the container is bent to the right. These effects are indications of susceptibility artefacts brought about by a mixture of the presence of paramagnetics and the various interfaces present in the sample [5,29]. These could be totally removed by using stronger applied magnetic field gradients (not possible with the instrument used in this study), but the effect seen here is not a major one. This is emphasised when, instead of looking directly at the image intensity, an intensity profile is examined. Figure 6 shows a profile measured along the section shown in Figure 5. The intensity distribution is uniform.

If the area containing oil is integrated, a measure of the intensity can be obtained. Figure 7 shows that a plot of the measured

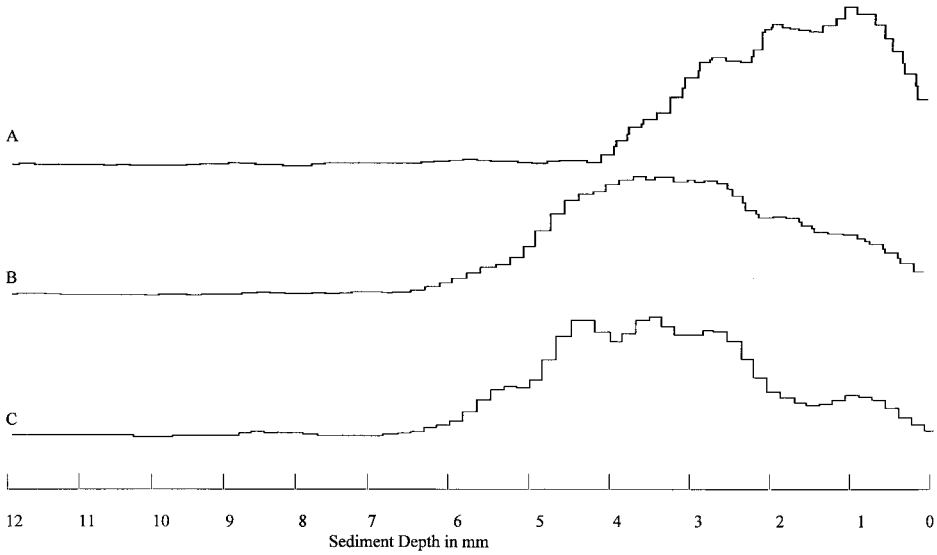

Figure 8 Three longitudinal profiles of image intensity down the central axis of a column of sediment contaminated from the top by dripping oil onto it. (A) The first hour after contamination; (B) after 36 h and (C) after 72 h.

intensity of a series of samples vs. the volume of oil added to the sediment in each is linear. This further justifies the use of this technique to follow oil movement in sediments.

As discussed above, the time needed to acquire images can be often be too long to give a meaningful result. Figure 4 shows an image of the container used to hold the sediment samples acquired using a $128\times32\times32$ data matrix. The reduction in time needed for the collection of these data allows oil diffusion to be measured over a meaningful time (1 h).

Using this acquisition protocol, movement of oil through the sediment can easily be measured. Figure 8 shows profiles of image intensity, which are a measure of oil density, along the central axis of the sediment column. Profile A, measured immediately after addition of the oil, shows a rounded profile. If the leading edge of the profile (the oil is moving down the column, to the left in the image) is visually examined, the sharp drop in intensity would indicate the diffusion in Case 2. However, the other profiles B and C, measured at 36 and 72 h, respectively, show that the diffusion is definitely Fician. It is likely that the initial profile (A) is more an indication of the effect of dripping oil on the sediment surface than a direct effect of diffusion.

By combining sample container with reference material, it has been demonstrated that MRI offers a new and important method for quantitatively assessing concentration (and potential movement) of oil in marine sediments, offering a method of determining the harming potential, in terms of the spread, of pollutant oils in the estuarine environment. Sacrifice of resolution in the transverse plane with maximum resolution in the longitudinal axis allows relatively rapid sample accumulation permitting dynamic changes to be followed. Such an analytical protocol could be used for calculating the extent to which longer-term remedial action is required when oil residues reach coastal areas by allowing the effects of pollution incidents to be understood in greater detail. Over succeeding years, improvements in environmental quality could be monitored, allowing recovery rates to be calculated.

Although in its infancy, the reported technique could lend itself well to the estimation of contaminant decay rates and provide a method for determining the effectiveness of bioremediation strategies.

References

1 Bech N, D Olsen and CM Neilsen. 2000. Determination of oil/water saturation functions of chalk core plugs from two-phase flow experiments. *SPE Reservoir Evaluation and Engineering* 3: 50–59.
2 Candela D, A Ding and XY Yang. 2000. Applications of NMR to transport in random systems. *Physica B* 279: 120–124.
3 Chang CTP and AT Watson. 1999. NMR imaging of flow velocity in porous media. *AIChE Journal* 45: 437–444.
4 Chudek JA and G Hunter. 1997. Magnetic resonance imaging in plants. In: Emsley JW and J Feeney (Eds.), Progress in NMR Spectroscopy, vol. 31, Pergamon, pp. 43–63.
5 Chudek JA and AD Reeves. 1998. An application of nuclear magnetic resonance imaging to study migration rates of oil-related residues in estuarine sediments. *Biodegradation* 9: 443–449.
6 Daughney CJ, TR Bryar and RJ Knight. 2000. Detecting sorbed hydrocarbons in a porous medium using proton nuclear magnetic resonance. *Environmental Science and Technology* 34: 332–337.
7 De Panfilis C and KJ Packer. 1999. Characterisation of porous media by NMR imaging and flow diffraction. *European Journal of Applied Physics* 8: 77–86.
8 Duval FP, P Porion and H VanDamme. 1999. Microscale and macroscale diffusion of water in colloid gels. A pulsed field and NMR imaging investigation. *Journal of Physical Chemistry* 103: 5730–5735.
9 Fukushima E. 1999. Nuclear magnetic resonance as a tool to study flow. *Annual Review of Fluid Mechanics* 31: 95–123.
10 Goelman G and MG Prammer. 1995. The CPMG pulse sequence in strong magnetic field gradients with applications to oil well logging. *Journal of Magnetic Resonance Series A* 113: 11–18.
11 Heitkamp MA, JP Freeman, DW Miller and CE Cerniglia. 1991. Biodegradation of 1-nitropyrene. *Archives of Microbiology* 156: 223–230.
12 Hoffman F, D Ronen and Z Pearl. 1996. Evaluation of flow characteristics of a sand column using magnetic resonance imaging. *Journal of Contaminant Hydrology* 22: 95–107.
13 Irwin NC, SA Altobelli, JH Cushman and RA Greenkorn. 1998. NMR imaging experiments for the verification of stochastic transport theory. *Magnetic Resonance Imaging* 16: 665–668.
14 Kogel-Knabner I. 1997. ^{13}C and ^{15}N NMR spectroscopy as a tool in soil organic matter studies. *Geoderma* 80: 243–270.

15 Kuhn W. 1990. NMR microscopy fundamentals, limits and possible applications. *Angewandte Chemie, International Edition in English* 29: 1–19.
16 Kulkarni R, AT Watson and JE Nordtvedt. 1998. Estimation of porous media flow functions using NMR imaging data. *Magnetic Resonance Imaging* 16: 707–709.
17 LaTorrace GA, KJ Dunn, PR Webber and RM Carlson. 1998. Low-field NMR determinations of the properties of heavy oils and water-in-oil emulsions. *Magnetic Resonance Imaging* 16: 659–662.
18 Lausen SK, H Lindgreen, HJ Jakobsen and NC Nielsen. 1999. Solid-state Si-29 MAS NMR studies of illite and illite–smectite from shale. *American Mineralogist* 84: 1433–1438.
19 Lens PNL and MA Hemminga. 1998. Nuclear magnetic resonance in environmental science and engineering: principles and applications. *Biodegradation* 9: 393–409.
20 Lindgreen H, H Jacobsen and HJ Jakobsen. 1991. Diagenetic structural transformations in north sea Jurassic illite–smectite. *Clays and Clay Minerals* 39: 54–69.
21 Maier RS, DM Kroll, HT Davis and RS Bernard. 1998. Pore scale flow and dispersion. *International Journal of Modern Physics C* 9: 1523–1533.
22 Mansfield P, R Bowler, S Blackbands and DN Guilfoyle. 1992. Magnetic resonance imaging applications of novel methods in the study of porous media. *Magnetic Resonance Imaging* 10: 741–746.
23 Manz B, P Alexander, PB Warren and LF Gladden. 1998. Characterisation of fluid flow through porous media using three-dimensional microimaging and pulsed gradient stimulated echo NMR. *Magnetic Resonance Imaging* 16: 673–675.
24 Manz B, LF Gladden and PB Warren. 1999. Flow and dispersion in porous media: Lattice–Boltzmann and NMR studies. *AIChE Journal* 45: 1845–1854.
25 Murgich J, M Corti, L Pavesi and F Voltini. 1992. Diffusion and spatially resolved NMR in Berea and Venezuelan oil reservoir rocks. *Magnetic Resonance Imaging* 10: 843–848.
26 Oswald S, W Kinzelbach, A Greiner and G Brix. 1997. Observation of flow and transport processes in artificial porous media via magnetic resonance imaging in three dimensions. *Geoderma* 80: 417–429.
27 Park J and SJ Gibbs. 1999. Mapping flow and dispersion in a packed column. *AIChE Journal* 45: 655–660.
28 Pervizpour M, S Pamukcu and H Moo-Young. 1999. Magnetic resonance imaging of hydrocarbon-contaminated porous media. *Journal of Computing in Civil Engineering* 13: 96–102.
29 Reeves AD and JA Chudek. 1998. Application of nuclear magnetic resonance imaging (MRI) to migration studies of oil residues in estuarine sediments (Tay Estuary). *Water Science and Technology* 38: 187–192.
30 Roy JL, WB McGill and MD Rawluk. 1999. Petroleum residues as water-repellent substances in weathered non-wettable oil-contaminated soils. *Canadian Soil Science* 79: 367–380.
31 Sardessai S and S Wahidullah. 1998. Structural characteristics of marine sedimentary humic acids by CP/MAS C-13 NMR spectroscopy. *Oceanologica Acta* 21: 543–550.
32 Stapf S and KJ Packer. 1998. Two-dimensional propagators and spatiotemporal correlations for flow in porous media. *Applied Magnetic Resonance* 15: 303–322.
33 VanAs H, W Palstra, U Tallarek and D VanDusschoten. 1998. Flow and transport studies in (non)consolidated porous (bio)systems consisting of solid or porous beads by PGF NMR. *Magnetic Resonance Imaging* 16: 569–573.
34 VanDusschoten D, D Tallarek, U Scheenen, T Neue and H VanAs. 1998. Spatially resolved transport properties in radially compressed bead packing studies by PGF NMR. *Magnetic Resonance Imaging* 16: 703–706.
35 Zhang YM, PC Xia and YJ Yu. 2000. Review of nuclear magnetic resonance magnet for oil well logging. *IEEE Transactions on Applied Superconductivity* 10: 763–766.
36 Zhou MY, DL Lu, J Dunsmuir and H Thomann. 2000. Irreducible water distribution in sandstone rock: two-phase flow simulations in CT-based pore network. *Physics and Chemistry of the Earth Part A* 25: 169–174.